LATTICE DYNAMICS
AND PHASE TRANSITIONS

Ab initio Calculations of Phonon Spectra in ATiO$_3$ Perovskite Crystals (A = Ca, Sr, Ba, Ra, Cd, Zn, Mg, Ge, Sn, Pb)

A. I. Lebedev

Moscow State University, Moscow, 119992 Russia
e-mail: swan@scon155.phys.msu.su
Received May 25, 2008

Abstract—First-principles calculations of phonon spectra based on the density functional theory are carried out for calcium, strontium, barium, radium, cadmium, zinc, magnesium, germanium, tin, and lead titanates with a perovskite structure. By analyzing unstable modes in the phonon spectrum, the possible types of lattice distortion are determined and the energies of the corresponding phases are calculated. From analyzing the phonon spectra, force constants, and eigenvectors of TO phonons, a conclusion is drawn concerning the nature of ferroelectric phenomena in the crystals studied. It is shown that the main factors determining the possible appearance of off-center atoms in the A position are the geometric size and electronic configuration of these atoms.

1. INTRODUCTION

Crystals of the perovskite family are well-known materials undergoing various structural distortions with decreasing temperature. When distortions are ferroelectric in character, a number of physical characteristics of the crystals (permittivity, piezoelectric coefficients, etc.) become anomalously large in magnitude. For this reason, these materials have found wide application in modern electronics.

The problem of further optimization of the properties of ferroelectrics requires a deep understanding of the microscopic mechanisms responsible for ferroelectricity and the appearance of these properties. In solving this problem, it is very helpful to further carry out ab initio calculations of physical properties of crystals, which have already made a significant contribution to the understanding of the ferroelectric phenomena in perovskite crystals [1–11].

In discussing the properties of ferroelectrics, it is very important to elucidate whether these properties result from collective displacements of atoms in the lattice (displacive phase transition) or they are determined by specific features of certain constituent atoms of the crystal (order–disorder phase transition). This problem arises, in particular, in discussing the nature of phase transitions that occur in incipient ferroelectrics doped with certain impurities [12].

Earlier studies of titanates with a perovskite structure have dealt mainly with four systems (CaTiO$_3$ [3, 4, 13, 14], SrTiO$_3$ [3, 4, 6], BaTiO$_3$ [1–4, 8, 9], and PbTiO$_3$ [2–4, 7, 9]) and solid solutions based on these compounds. However, a comparison of the obtained results is hampered by the fact that those studies differ in terms of calculation techniques and methods used to construct atomic potentials.

The objective of this work is to carry out first-principles calculations of the phonon spectra of ten ATiO$_3$ crystals with a perovskite structure and determine the structure of the stable phases for these crystals. In order to test the method used, we first apply it for calculating the properties of the four systems mentioned above and then we study the properties of poorly investigated or hypothetical perovskite crystals RaTiO$_3$, CdTiO$_3$, MgTiO$_3$, ZnTiO$_3$, SnTiO$_3$, and GeTiO$_3$. From comparing the results obtained in a unified way for a large number of related materials, conclusions are inferred concerning the relation of the structural distortions in the ATiO$_3$ crystals to the size of the A atom and its electronic structure. From analyzing the on-site force-constant matrix elements and the TO-phonon eigenvectors, we draw conclusions regarding the nature of ferroelectric phenomena in these materials and find conditions under which these phenomena can be associated with off-center atoms.

2. CALCULATION TECHNIQUE

The calculations are carried out using the ABINIT software [15] based on the density functional theory, pseudopotentials, and expansions of the wave functions in plane waves. The exchange-correlation interaction is described in the local-density approximation (LDA) using the technique developed in [16]. The pseudopo-

Table 1. Electronic configurations of atoms and parameters used to construct pseudopotentials: r_s, r_p, and r_d are the core radii of the pseudopotentials for the s, p, and d projections; q_s, q_p, and q_d are the limiting values of wave vectors used to optimize pseudopotentials; and r_{min}, r_{max}, and V_{loc} are the range limits and the depth of the correcting local potential (parameter values are in atomic units, and energy is given in Ry)

Atom	Configuration	r_s	r_p	r_d	q_s	q_p	q_d	r_{min}	r_{max}	V_{loc}
Ca	$3s^2 3p^6 3d^0 4s^0$	1.46	1.68	1.82	7.07	7.07	7.27	0.01	1.40	1.6
Sr	$4s^2 4p^6 4d^0 5s^0$	1.68	1.74	1.68	7.07	7.07	7.07	0.01	1.52	1.5
Ba	$5s^2 5p^6 5d^0 6s^0$	1.85	1.78	1.83	7.07	7.07	7.07	0.01	1.68	1.95
Ra	$6s^2 6p^6 7s^0 6d^0 7p^0$	1.84	1.73	1.98	7.8	7.8	7.8	0.01	1.68	−1.3
Mg	$2s^2 2p^6 3s^0 3p^0$	1.50	1.88	–	6.7	8.1	–	0.01	1.0	−0.84
Zn	$3d^{10} 4s^0 4p^0$	1.82	1.82	2.00	7.07	7.07	7.47	0.01	1.60	2.5
Cd	$4d^{10} 5s^0 5p^0$	2.04	2.18	2.10	7.07	7.07	7.07	0	1.88	−1.6
Ge	$3d^{10} 4s^{1.5} 4p^{0.5}$	1.68	1.68	1.96	7.07	6.0	7.77	0.01	1.58	0.48
Sn	$4d^{10} 5s^2 5p^0$	2.14	2.08	2.18	7.07	7.07	7.07	0.01	1.90	0.64
Pb	$5d^{10} 6s^2 6p^0$	1.80	1.72	1.98	6.05	5.52	7.17	0.1	1.43	1.6
Ti	$3s^2 3p^6 3d^0 4s^0$	1.48	1.72	1.84	7.07	7.07	7.07	0.01	1.41	2.65
O	$2s^2 2p^2 3d^0$	1.40	1.55	1.40	7.07	7.57	7.07	–	–	–

tentials used are optimized separable nonlocal pseudopotentials [17], which are constructed using the OPIUM computer program and to which a local potential is added according to [18] in order to improve their transferability. The calculations for elements with atomic numbers $Z < 46$ are performed without inclusion of relativistic effects; for other elements, a scalar relativistic approximation is used. Table 1 lists the parameters used for constructing pseudopotentials. The local potential is chosen to be an s potential, except for oxygen atoms, for which a local d potential is used. The parameters of pseudopotentials are finely adjusted by comparing the computed and experimental values of lattice parameters for a number of oxides and sulfides of elements.

The lattice parameters and the equilibrium atomic positions in the unit cell are found by minimizing the Hellmann–Feynman forces acting on the atoms ($<10^{-5}$ Ha/Bohr), with the total crystal energy being calculated self-consistently with an accuracy of better than 10^{-10} Ha.[1] In calculations, particular attention is given to the convergence of the results with respect to the choice of the cut energy of plane waves and the fineness of the grid of wave vectors used in integration over the Brillouin zone. For all the computed quantities that are discussed below, the convergence is attained with a cut energy of 30 Ha and with a $8 \times 8 \times 8$ grid constructed according to [19].

Effective charges Z^*, optical dielectric constant ε_∞, elastic moduli C_{ij}, bulk modulus B, force-constant matrix Φ_{ij}, and phonon spectra are calculated using perturbation theory [20–23]. The phonon energies are

exactly calculated at five points of the Brillouin zone (Γ, X, M, R, and the Λ point located halfway between the Γ and R points), and then the phonon spectrum is computed over the entire Brillouin zone using the interpolation technique described in [20, 24].

3. TESTING OF THE CALCULATION TECHNIQUE

The correctness of the calculation technique described above is tested by comparing the calculated lattice parameters, spontaneous polarization, and phonon spectra with the available experimental data and calculations performed by other authors for well-studied CaTiO_3, SrTiO_3, BaTiO_3, and PbTiO_3.

The lattice parameter values corresponding to a minimum total energy of the crystal are listed in Table 2. These computed values agree well with the experimental data from [25] if we take into account that the LDA systematically slightly underestimates the lattice parameters. An analysis of the relative energies (per formula unit) of the low-symmetry phases (Table 3) shows that the energetically most favorable phase for barium titanate is the rhombohedral phase and, for lead titanate, the tetragonal phase. The calculated values of the ratio c/a for tetragonal BaTiO_3 and tetragonal PbTiO_3 are close to the experimental values (Table 2). In CaTiO_3, the energetically most favorable phase is the orthorhombic phase $Pbnm$ and, in SrTiO_3, the tetragonal phase $I4/mcm$. The values of the spontaneous polarization calculated by the Berry phase method [26] are 0.26, 0.31, and 0.89 C/m² for tetragonal BaTiO_3, rhombohedral BaTiO_3, and PbTiO_3, respectively. These values are close to experimental data (0.26, 0.33, 0.75 C/m² [25]).

---

[1] In this paper, the energy is measured in the Hartree atomic system of units (1 Ha = 27.2113845 eV) everywhere except in Tables 1 and 3.

Table 2. Comparison of calculated and experimental crystal lattice parameters of various phases of $ATiO_3$ compounds (experimental data are obtained at 300 K, unless otherwise specified)

Compound	Space group	Source	Lattice parameters
CaTiO$_3$	Pbnm	This work	$a = 5.3108$ Å, $b = 5.4459$ Å, $c = 7.5718$ Å
		Expt. [25]	$a = 5.3670$ Å, $b = 5.4439$ Å, $c = 7.6438$ Å
SrTiO$_3$	Pm3m	This work	$a = 3.8898$ Å
		Expt. [25]	$a = 3.905$ Å
	I4/mcm	This work	$a = b = 5.4680$, $c = 7.8338$ Å
		Expt. [25]	$a = b = 5.510$, $c = 7.798$ Å (20 K)
BaTiO$_3$	Pm3m	This work	$a = 3.9721$ Å
		Expt. [25]	$a = 3.996$ Å (393 K)
	P4mm	This work	$a = 3.9650$, $c = 4.0070$ Å, $c/a = 1.0106$
		Expt. [25]	$a = 3.9920$, $c = 4.0361$ Å (293 K)
	Amm2	This work	$a = 3.9620$, $b = 5.6384$, $c = 5.6484$ Å
		Expt. [25]	$a = 3.990$, $b = 5.669$, $c = 5.682$ Å (263 K)
	R3m	This work	$a = 3.9817$ Å, $\alpha = 89.933°$
		Expt. [25]	$a = 4.001$ Å, $\alpha = 89.85°$ (105 K)
PbTiO$_3$	P4mm	This work	$a = 3.8858$, $c = 4.1151$ Å, $c/a = 1.0590$
		Expt. [25]	$a = 3.904$, $c = 4.152$ Å

The calculated optical-phonon energies are also in good agreement with available experimental data and calculations performed by other authors (Tables 4, 5). The imaginary frequencies (negative squares of the frequencies) in Tables 4 and 5 correspond to unstable modes.

The good agreement of our calculations with the experimental data and the calculation results of other authors for CaTiO$_3$, SrTiO$_3$, BaTiO$_3$, and PbTiO$_3$ suggests that we can use the proposed calculation technique to predict the properties of poorly studied and hypothetical[2] perovskite titanates and analyze the factors causing the appearance of ferroelectricity in these crystals. Tables 3–7 show the characteristics of these crystals calculated for the theoretical value of the lattice parameter (i.e., the value corresponding to a minimum of the total energy). Table 3 lists the energies of several low-symmetry phases of the crystals measured relative to the energy of the original cubic phase. Table 4 gives the frequencies of optical phonons (six infrared-active Γ_{15} modes and one infrared-inactive Γ_{25} mode) in the cubic phase of the same crystals, and Table 5 gives the lowest phonon energies at high-symmetry points of the Brillouin zone. Table 6 lists the values of the effective charges and optical dielectric constant for the cubic phase of the $ATiO_3$ compounds. Finally, Table 7 gives the elastic moduli of several crystals.

The phonon spectra along certain directions calculated for the cubic phase of the ten titanates studied are shown in Fig. 1. The imaginary phonon energies associated with structural instability of the crystals are represented in Fig. 1 by negative numbers.

4. RESULTS

It follows from Fig. 1 that the phonon spectra of all titanates studied have unstable optical modes of different symmetry. First, we discuss the phonon spectra of well-studied crystals.

A specific feature of the dispersion curves of SrTiO$_3$ is that, out of three unstable phonons at the Γ, R, and M points, the most unstable is the phonon at the R point (R_{25} mode)[3] and that the phonon energy depends only slightly on wave vector along the R–M line. As shown in [6], in the real space, these unstable phonons with wave vectors near the edges of the cubic Brillouin zone correspond to rotation of oxygen octahedra linked together by shared vertices, with a correlation length of this rotation being three to five lattice periods. Thus, the R_{25} mode and the M_3 mode (which corresponds to the unstable phonon at the M point) describe structural distortions associated with rotation of the octahedra. The unstable Γ_{15} phonon mode at the Γ point corresponds to ferroelectric distortions of the crystal structure.

The R_{25} mode is threefold degenerate, and distortions described by three-component order parameters $(\eta, 0, 0)$, $(\eta, \eta, 0)$, and (η, η, η) lead to low-symmetry

---

[2] Our calculations show that the energy of the ilmenite phase of SnTiO$_3$, GeTiO$_3$, CdTiO$_3$, ZnTiO$_3$, and MgTiO$_3$ at $T = 0$ is lower than the energy of the most stable of the distorted perovskite phases. However, only for the two last crystals is the difference between these phases large (0.30–0.33 eV).

[3] We use the mode notation introduced in [29].

Table 3. Relative energies of various low-symmetry phases of ATiO$_3$ compounds (energies of the most stable phases are in boldface)

Compound	Unstable mode	Space group	Energy, meV	Unstable mode	Space group	Energy, meV
MgTiO$_3$	X'_5	$Cmcm$	−304	M_3	$P4/mbm$	−1107
	X'_5	$Pmma$	−500	R_{25}	$I4/mcm$	−1111
	Γ_{15}	$R3m$	−695	R_{25}	$R\bar{3}c$	−1727
	Γ_{15}	$P4mm$	−1028	$R_{25} + M_3$	$Pbnm$	**−1992**
CaTiO$_3$	X'_5	$Cmcm$	−0.6	Γ_{15}	$P4mm$	−123
	X'_5	$Pmma$	−0.9	M_3	$P4/mbm$	−321
	M'_5	$Pmma$	−5.0	R_{25}	$I4/mcm$	−365
	M'_5	$Cmmm$	−6.7	R_{25}	$R\bar{3}c$	−385
	Γ_{15}	$R3m$	−73.7	$R_{25} + M_3$	$Pbnm$	**−497**
SrTiO$_3$	Γ_{15}	$P4mm$	−0.71	R_{25}	$R\bar{3}c$	−27.5
	Γ_{15}	$R3m$	−0.75	$R_{25} + M_3$	$Pbnm$	−28.9
	M_3	$P4/mbm$	−9.45	R_{25}	$I4/mcm$	**−30.9**
BaTiO$_3$	M'_3	$P4/nmm$	−0.31	Γ_{15}	$P4mm$	−5.6
	X_5	$Pmma$	−1.22	Γ_{15}	$Amm2$	−7.4
	X_5	$Cmcm$	−1.45	Γ_{15}	$R3m$	**−8.1**
RaTiO$_3$	M'_3	$P4/nmm$	−11.1	Γ_{15}	$P4mm$	−21.8
	X_5	$Pmma$	−14.2	Γ_{15}	$Amm2$	−28.5
	X_5	$Cmcm$	−16.9	Γ_{15}	$R3m$	**−29.7**
CdTiO$_3$	X_3	$P4_2/mmc$	−45	Γ_{15}, Γ_{25}	$Amm2$	−412
	Γ_{25}	$P\bar{4}m2$	−134	Γ_{25}	$R32$	−486
	X_5	$Pmma$	−160	R_{25}	$I4/mcm$	−912
	Γ_{15}	$R3m$	−245	M_3	$P4/mbm$	−920
	X_5	$Cmcm$	−282	R_{25}	$R\bar{3}c$	−1197
	Γ_{15}	$P4mm$	−340	$R_{25} + M_3$	$Pbnm$	**−1283**
ZnTiO$_3$	Γ_{25}	$P\bar{4}m2$	−341	R_{25}	$I4/mcm$	−1443
	X_5	$Pmma$	−447	M_3	$P4/mbm$	−1449
	X_5	$Cmcm$	−867	Γ_{25}	$R32$	−1486
	Γ_{15}	$R3m$	−868	R_{25}	$R\bar{3}c$	−2271
	Γ_{15}	$P4mm$	−1104	$R_{25} + M_3$	$Pbnm$	**−2312**
	Γ_{15}, Γ_{25}	$Amm2$	−1254			
GeTiO$_3$	X'_5	$Pmma$	−328	R_{25}	$R\bar{3}c$	−589
	X'_5	$Cmcm$	−428	$R_{25} + M_3$	$Pbnm$	−810
	M_3	$P4/mbm$	−444	Γ_{15}	$P4mm$	−854
	R_{25}	$I4/mcm$	−455	Γ_{15}	$R3m$	**−1053**
SnTiO$_3$	X'_5	$Pmma$	−21	R_{25}	$R\bar{3}c$	−74
	X'_5	$Cmcm$	−23	$R_{25} + M_3$	$Pbnm$	−84
	M_3	$P4/mbm$	−57	Γ_{15}	$R3m$	−240
	R_{25}	$I4/mcm$	−67	Γ_{15}	$P4mm$	**−291**
PbTiO$_3$	M_3	$P4/mbm$	−10.1	$R_{25} + M_3$	$Pbnm$	−22.2
	R_{25}	$I4/mcm$	−19.6	Γ_{15}	$R3m$	−66.3
	R_{25}	$R\bar{3}c$	−21.6	Γ_{15}	$P4mm$	**−84.4**

Table 4. Frequencies of optical phonons at the Γ point in the cubic phase of ATiO$_3$ compounds (in cm^{-1})

Compound	Source	TO1	TO2	TO3	LO1	LO2	LO3	Γ_{25}
MgTiO$_3$	This work	260i	151	649	106i	372	905	191i
CaTiO$_3$	Same	165i	176	607	122	407	857	93
	Calc. [3]	153i	188	610	133	427	866	–
	Calc. [13]	140i	200	625	136	428	864	130
SrTiO$_3$	This work	68i	162	549	152	428	792	202
	Calc. [3]	41i	165	546	158	454	829	–
	Calc. [6]	100i	151	522	146	439	751	219
	Expt. [27]	–	175	544	172	475	796	–
BaTiO$_3$	This work	151i	175	471	172	439	683	269
	Calc. [3]	178i	177	468	173	453	738	–
	Calc. [8]	195i	166	455	162	434	657	266
	Expt. [28]^a	–	181	487	180	468	717	306
RaTiO$_3$	This work	212i	172	444	166	434	638	287
ZnTiO$_3$	This work	240i	76	645	105i	316	815	353i
CdTiO$_3$	Same	187i	97	616	34	353	820	231i
GeTiO$_3$	This work	247i	122	583	68i	356	762	49i
SnTiO$_3$	Same	185i	126	505	80	375	689	183
PbTiO$_3$	″	150i	116	499	96	394	693	202
	Calc. [3]	144i	121	497	104	410	673	–
	Calc. [7]	182i	63	447	47	418	610	–

Note: ^{a} Data for the tetragonal phase.

phases belonging to space groups *I4/mcm*, *Imma*, and $R\bar{3}c$, respectively. The M_3 mode is nondegenerate, and its condensation reduces the crystal symmetry to *P4/mbm*. The threefold degenerate Γ_{15} mode is described by space groups *P4mm*, *Amm2*, and *R3m*. From comparing the energies of these phases (Table 3),[4] it follows that the lowest energy phase of SrTiO$_3$ is the *I4/mcm* phase, which arises with decreasing temperature. The instability of the ferroelectric mode is not sufficiently strong for ferroelectricity to occur in the crystal.

In CaTiO$_3$, in addition to the instabilities indicated above, three weak antiferroelectric-type instabilities arise associated with the X_5, X_5', and M_5' modes and the R–M segment of the phonon spectrum is practically dispersionless (cf. mode energies in Table 5). In the latter case, theoretical calculations showed [14] that the simultaneous condensation of the unstable R_{25} and M_3 modes brings about the formation of a low-temperature *Pbnm* phase having the lowest energy among the possible distorted phases (Table 3).[5] The transition from the high-temperature *Pm3m* phase to the *Pbnm* phase can

occur through one of three intermediate phases (*P4/mbm*, *I4/mcm*, and $R\bar{3}c$), whose energies are 0.11–0.17 eV higher than the energy of the *Pbnm* phase. The ferroelectric *P4mm* and *R3m* phases in CaTiO$_3$ have far higher energies and never arise. As for the weakly unstable X_5', X_5, and M_5' modes, they are twofold degenerate and distortions described by the order parameters $(\eta, 0)$ and (η, η) lead to the *Pmma*, *Cmcm*, and *Cmmm* phases. However, the energy gained in the transformation into these phases does not exceed 7 meV.

The phonon spectrum of BaTiO$_3$ differs significantly from the spectra discussed above by the absence of instability at the R point and the appearance of highly unstable X_5 and M_3' modes (at the X and M points, respectively) corresponding to ferroelectric transformations into the *Pmma*, *Cmcm*, and *P4/nmm* phases. Among these modes, the most unstable is the ferroelectric Γ_{15} mode and this mode determines crystal distortions (the three antiferroelectric phases are higher in energy than the polar *P4mm* phase). We note that, in our

---

[4] We do not present in the table the energies of phases described by the order parameter $(\eta, \eta, 0)$, because these phases arise in the rare case when the coefficient of the second fourth-order invariant constructed from the order parameter components becomes zero.

[5] Calculations show that, in SrTiO$_3$, despite the presence of the unstable R_{25} and M_3 modes in the phonon spectrum, the energy of the *Pbnm* phase is 2 meV higher than that of the *I4/mcm* phase.

Table 5. Lowest phonon frequencies at high-symmetry points of the Brillouin zone in the cubic phase of ATiO$_3$ compounds (in cm^{-1})

Com-pound	Source	Γ	X	M	R	Λ
MgTiO$_3$	This work	260i	190i	314i	315i	246i
CaTiO$_3$	Same	165i	32i	215i	226i	122i
	Calc. [13]	140i	20	207i	219i	–
SrTiO$_3$	This work	68i	98	86i	119i	100
BaTiO$_3$	Same	151i	96i	59i	134	105
	Calc. [8]	219i	189i	167i	128	–
RaTiO$_3$	This work	212i	182i	158i	110	87
ZnTiO$_3$	This work	353i[a]	319i	437i	424i	337i
CdTiO$_3$	Same	231i[a]	184i	333i	328i	265i
GeTiO$_3$	This work	247i	148i	254i	251i	201i
SnTiO$_3$	Same	185i	56i	144i	148i	97i
PbTiO$_3$	"	150i	30	96i	113i	15i
	Calc. [7]	182i	31i	35i	145i	58i

Note: [a] Γ_{25} mode.

Table 6. Effective charges and optical dielectric constant for the cubic phase of ATiO$_3$ compounds

Compound	Z_A^*	Z_{Ti}^*	$Z_{O\perp}^*$	$Z_{O\parallel}^*$	ε_∞
MgTiO$_3$	2.537	7.773	–2.026	–6.258	7.01
CaTiO$_3$	2.579	7.692	–2.085	–6.101	6.84
SrTiO$_3$	2.561	7.725	–2.099	–6.088	6.87
BaTiO$_3$	2.738	7.761	–2.186	–6.128	7.28
RaTiO$_3$	2.764	7.789	–2.181	–6.192	7.42
ZnTiO$_3$	3.233	8.257	–2.427	–6.637	11.64
CdTiO$_3$	3.040	8.052	–2.300	–6.493	9.35
GeTiO$_3$	4.460	7.572	–2.860	–6.314	10.49
SnTiO$_3$	4.255	7.529	–2.745	–6.294	10.18
PbTiO$_3$	3.931	7.623	–2.635	–6.283	9.34

calculations, the phonons in BaTiO$_3$ are less unstable than in the calculations performed in [9], because we used the theoretical value of the lattice parameter, whereas the calculations in [9] were performed for the experimental value of this parameter. The dependence of the phonon spectrum on the lattice parameter is illustrated in Fig. 1, wherein the dotted line shows a fragment of the phonon spectrum of BaTiO$_3$ calculated with the same lattice parameter as that in [9].

The weak dependence of the energy of the unstable TO phonon on wave vector along the Γ–X–M–Γ line for vibrations polarized along the fourfold axes of the cubic lattice was first discovered in [5]. This dependence shows that the linear chains …–O–Ti–O–… oriented along these axes dominate in the vibrations and that the interaction between the parallel chains is weak.

A comparison of the phonon spectra of BaTiO$_3$ and RaTiO$_3$ shows that these spectra are very similar. In radium titanate, the most unstable is the Γ_{15} mode, whose energy depends only slightly on wave vector along the Γ–X–M–Γ line and the instability of phonons is even more pronounced than in BaTiO$_3$. Taking into account the calculated energies of the distorted phases (Table 3), we can assume that RaTiO$_3$ is also a ferroelectric and that, as the temperature decreases, it successively undergoes three phase transitions as barium titanate does. The temperatures of these transitions are likely to be higher than those in barium titanate. The values of the spontaneous polarization in RaTiO$_3$ as calculated by the Berry phase method are also higher than those in BaTiO$_3$ and are 0.36 C/m^2 in the tetragonal phase and 0.41 C/m^2 in the rhombohedral phase.

The calculated elastic moduli of the cubic RaTiO$_3$ are given in Table 7.

Now, we consider the phonon spectrum of CdTiO$_3$. This spectrum has a number of unstable modes at the X, M, and R points (X_3, X_5, X_5', M_3, M_5', M_2', R_{25}, R_{15} modes) and two unstable modes at the Γ point. It is surprising that the instability at the Γ point is due to the Γ_{25} mode associated with deformation of the oxygen octahedron (see mode energies in Table 4) rather than to the ferroelectric Γ_{15} mode. Such a deformation can bring about the formation of the $P\bar{4}m2$, $Amm2$, and $R32$ phases, depending on the number of nonzero order parameter components.[6] The energy of the most stable of these phases ($R32$, Table 3) is lower than that of the polar phases. Due to the qualitative similarity between the phonon spectra of calcium and cadmium titanates and between the eigenvectors of their unstable modes at the R and M points, CdTiO$_3$ can be considered an analog of CaTiO$_3$, but characterized by a higher instability. Therefore, at room temperature, the nonpolar phase has $Pbnm$ symmetry, as is the case for CaTiO$_3$. This conclusion was also drawn in [30]. However, according to our data, the energy of this phase is lower than that of the cubic phase by 1.28 eV (Table 3), which is somewhat greater than the value obtained in [30] (0.8 eV) and [10] (0.91 eV).

The ferroelectric instability associated with the Γ_{15} mode is not of great importance in the cubic CdTiO$_3$, but it is known that this instability manifests itself in the $Pbnm$ phase and leads to a ferroelectric phase transition at 80 K. The first-principles calculations of the properties of the orthorhombic CdTiO$_3$ performed in [30] did

---

[6] The fact that the lattice symmetry can be lowered to the polar $Amm2$ group follows from the transformation properties of the order parameter (η, η, 0). The spontaneous polarization in this phase is 0.018 C/m^2.

Table 7. Elastic moduli of the cubic phase of $ATiO_3$ compounds (in GPa)

Compound	Source	C_{11}	C_{12}	C_{44}	B
$CaTiO_3$	This work	388	100	91	196
	Calc. [4]	407	96	101	200
$SrTiO_3$	This work	373	103	108	193
	Calc. [4]	388	104	117	199
	Expt. [25]	316–348	101–103	119–124	174–183
$BaTiO_3$	This work	338	110	123	186
	Calc. [4]	329	117	130	188
$RaTiO_3$	This work	319	112	126	181
$PbTiO_3$	Same	336	127	95	197
	Calc. [4]	334	145	100	208
	Calc. [7]	320	141	375?	201

not revealed a stable ferroelectric distortion in it. In contrast to the calculations in [30], our calculations of the phonon spectrum of the orthorhombic $CdTiO_3$ at the Γ point revealed two unstable B_{1u} and B_{2u} modes causing the formation of polar $Pb2_1m$ and $Pbn2_1$ phases, respectively. Such lattice distortions have been detected by X-ray studies of cadmium titanate at low temperatures [31, 32]. We will discuss the properties of these phases in a later paper.

The phonon spectrum of $ZnTiO_3$ is qualitatively similar to that of $CdTiO_3$, but it has an additional weak unstable M'_3 mode and is less stable. Moreover, the Γ_{25} mode is less stable that the Γ_{15} mode in it (Table 4). However, the most unstable are the R_{25} and M_3 modes and, therefore, the $Pbnm$ phase is energetically most favorable in $ZnTiO_3$ as well (Table 3). The calculations of the phonon spectrum at the Γ point of the orthorhombic zinc titanate revealed two unstable B_{1u} and B_{2u} modes, which cause the formation of the same polar phases as those in cadmium titanate.

The phonon spectrum of $MgTiO_3$ is intermediate between those of zinc titanate and calcium titanate. It likewise has unstable Γ_{15} and Γ_{25} modes, but the ferroelectric Γ_{15} mode is lower in energy in magnesium titanate (Table 4). However, the phonons at the R and M points have the lowest energy and, therefore, the $Pbnm$ phase is energetically most favorable (Table 3). The calculations of the phonon spectrum of the orthorhombic magnesium titanate at the Γ point revealed one unstable B_{1u} mode that can cause a $Pbnm \longrightarrow Pbn2_1$ ferroelectric phase transition.

Finally, let us discuss the phonon spectra of $PbTiO_3$, $SnTiO_3$, and $GeTiO_3$. The ferroelectric instability of these three crystals is associated with the Γ_{15} mode, which competes with the unstable R_{25} and M_3 modes. From comparing the energies of various distorted phases (Table 3), it follows that, even in $GeTiO_3$,

wherein the unstable phonons at the Γ, R, and M points are close in frequency, the ferroelectric instability is dominant. The calculated spontaneous polarization is 1.28 C/m^2 in the tetragonal $SnTiO_3$ and 1.37 C/m^2 in the rhombohedral $GeTiO_3$. Our value of the spontaneous polarization in $SnTiO_3$ is significantly greater than the value 0.73 C/m^2 obtained in [33]. Among the perovskite crystals studied to date, $GeTiO_3$ is likely to have the highest spontaneous polarization.

It is worth noting that, in $PbTiO_3$ and $SnTiO_3$, the energetically most favorable is the tetragonal $P4mm$ phase and, in $GeTiO_3$, the rhombohedral $R3m$ phase. In the tetragonal $GeTiO_3$, the lattice deformation ($c/a = 1.1821$) is far greater than that in lead titanate ($c/a = 1.0590$). This result casts doubt on the conclusion inferred in [2] that the tetragonal phase stabilizes due to a large lattice deformation (large value of the ratio c/a).

5. DISCUSSION

As follows from Fig. 1, the phonon spectra of all $ATiO_3$ perovskite crystals studied have several unstable modes, among which there is always the ferroelectric Γ_{15} mode. In the case where the R_{25} and M_3 modes competing with it have a lower energy, the crystal undergoes distortions like octahedron rotation and the lattice symmetry is lowered to $I4/mcm$ or $Pbnm$. The tendency toward such structural phase transitions increases with decreasing A atom size.

From analyzing the characteristics of the Γ_{15} mode, one can draw a conclusion concerning the nature of the ferroelectric instability of the crystals. As mentioned above, the dispersion law of this mode in $BaTiO_3$ and $RaTiO_3$ indicates strongly correlated motions of atoms along chains …–O–Ti–O–…. An analysis of the eigenvectors corresponding to the Γ_{15} phonon (Table 8) shows that the A atoms are indeed involved in the motion only slightly and the motion is mainly due to
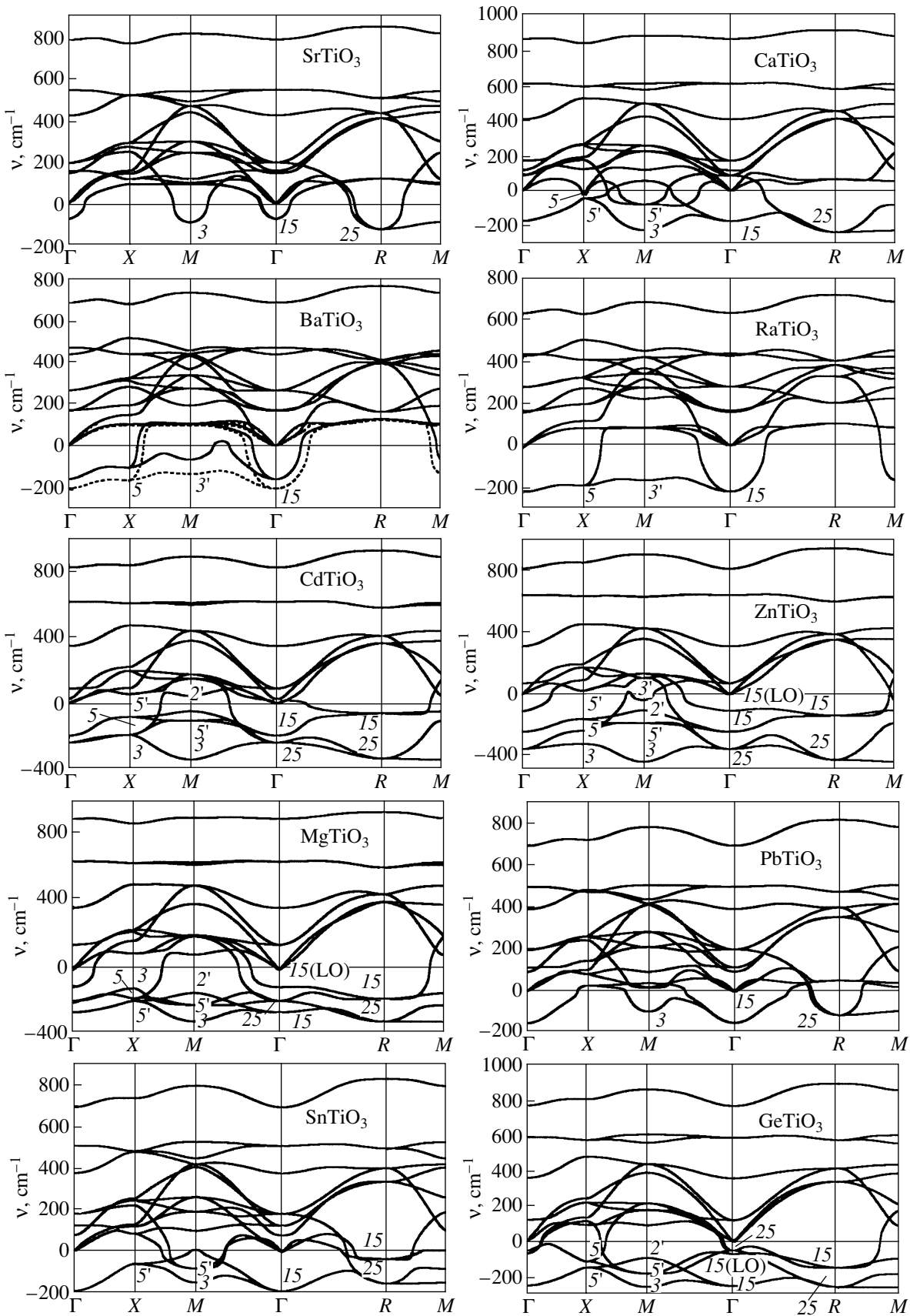
Fig. 1. Phonon spectra of the cubic phase of ATiO$_3$ compounds. The symmetry of the unstable modes is indicated near the curves.

Table 8. Eigenvectors of the dynamic matrix corresponding to an unstable TO1 phonon at the Γ point for the cubic phase of ATiO$_3$ compounds

Compound	x_A	x_{Ti}	$x_{O\perp}$	$x_{O\parallel}$
MgTiO$_3$	+0.6828	+0.1831	−0.4800	−0.1985
CaTiO$_3$	+0.5693	+0.2391	−0.5225	−0.2696
SrTiO$_3$	+0.3434	+0.3852	−0.5372	−0.3956
BaTiO$_3$	+0.0299	+0.6734	−0.3561	−0.5404
RaTiO$_3$	+0.0051	+0.6750	−0.2841	−0.6188
ZnTiO$_3$	+0.5167	+0.1889	−0.5655	−0.2403
CdTiO$_3$	+0.4012	+0.2358	−0.5919	−0.2875
GeTiO$_3$	+0.5367	+0.1382	−0.5573	−0.2677
SnTiO$_3$	+0.4177	+0.2123	−0.5670	−0.3709
PbTiO$_3$	+0.2973	+0.2865	−0.5675	−0.4305

Table 9. Diagonal elements $\Phi_{xx}(0, 0)$ of the on-site force-constant matrix for A and Ti atoms in the cubic phase of ATiO$_3$ compounds (in Ha/Bohr^2)

Compound	A atom	Ti atom
MgTiO$_3$	−0.0109	+0.1431
CaTiO$_3$	+0.0163	+0.1370
SrTiO$_3$	+0.0445	+0.1196
BaTiO$_3$	+0.0755	+0.0873
RaTiO$_3$	+0.0856	+0.0750
ZnTiO$_3$	−0.0229	+0.1072
CdTiO$_3$	−0.0008	+0.1113
GeTiO$_3$	−0.0150	+0.0949
SnTiO$_3$	+0.0132	+0.0786
PbTiO$_3$	+0.0269	+0.0803

antiphase Ti and O$_\parallel$ displacements. As the A atoms decrease in size, their contribution to the motion increases and becomes dominant, whereas the contribution from the Ti atoms decreases and the antiphase motion involves not O$_\parallel$ but O$_\perp$ displacements. Thus, in crystals with small A atoms, the ferroelectric mode involves antiphase displacements of A atoms and oxygen cuboctahedra.

Table 9 gives the values of the diagonal elements $\Phi_{xx}(0, 0)$ of the "on-site" force-constant matrix for the A and Ti atoms. These matrices are defined in terms of the restoring force acting on an atom displaced from the site, with the other atoms remaining fixed at their sites. In order to determine the on-site force constants from the force constants calculated using the ABINIT software for a crystal sublattice displaced as a unit, we average the force constants found for a regular grid of wave vectors [20, 22, 24]. Positive values of the on-site force constants indicate that the position of the atom at the site is stable, and negative values indicate that an off-center atom is formed. It follows from Table 9 that off-center A atoms arise in ATiO$_3$ perovskites for Mg, Zn, Cd, and Ge. The Sn, Ca, and Pb atoms are fairly close to the boundary of stability against the transition to an off-center position.

It will be recalled that the calculations in this paper are performed for the theoretical lattice parameter (corresponding to a minimum of the total crystal energy). Since the lattice parameters are systematically underestimated in LDA, which makes the ferroelectric instability weaker, many authors perform calculations using the experimental lattice parameter values. In order to estimate the influence of this systematic error, we carried out a computer simulation, which showed that a 1% increase in the lattice parameter (which is a typical error of LDA calculations) decreases $\Phi_{xx}(0, 0)$ in PbTiO$_3$ by 0.006 Ha/Bohr^2 for the A atom and by 0.016 Ha/Bohr^2 for the Ti atom. As a result, the atoms

positioned near the boundary of stability against the transition to an off-center position remain actually at their sites. Perhaps, this is the case in lead titanate, as indicated by extended X-ray-absorption fine-structure (EXAFS) studies [34].

The main parameter determining the tendency for the A atom in ATiO$_3$ crystals to transfer to an off-center position is the A atomic size. As can be seen from the dependences of the diagonal element $\Phi_{xx}(0, 0)$ of the force-constant matrix of the A atom on its ionic radius shown in Fig. 2, these dependences for Zn and Cd atoms, as well as for Ge, Sn, and Pb atoms, differ from those for the main series of Mg–Ca–Sr–Ba–Ra. The difference is likely due to the different electronic configurations of the filled atomic shells. This configuration is d^{10} for Zn and Cd; $d^{10}s^2$ for Ge, Sn, and Pb; and s^2p^6 for the atoms of the main series. The difference in the properties of these groups of atoms is also clearly manifested in the values of the effective charges of the A atoms (Table 6). Indeed, for the main series, the effective charge Z_A^* differs only slightly from the nominal cationic charge (which indicates that the A–O bond is mainly ionic); for the other two groups, the charge Z_A^* is significantly greater, which indicates that the bonding becomes more covalent in character [3].

These results suggest that off-center impurity atoms can exist in solid solutions of titanates with a perovskite structure. Since the average interatomic distance in such crystals is determined by the matrix, one might expect, according to the dependences discussed above, that the atoms for which $\Phi_{xx}(0, 0)$ has negative or small positive values will be in off-center positions. Therefore, it is likely that the ferroelectric phase transition induced by Ca, Cd, and Pb impurity atoms in SrTiO$_3$ [12] is due to the fact that these atoms are in off-center positions. According to EXAFS data, Ba impurity atoms in SrTiO$_3$ are not in off-center positions [35], but
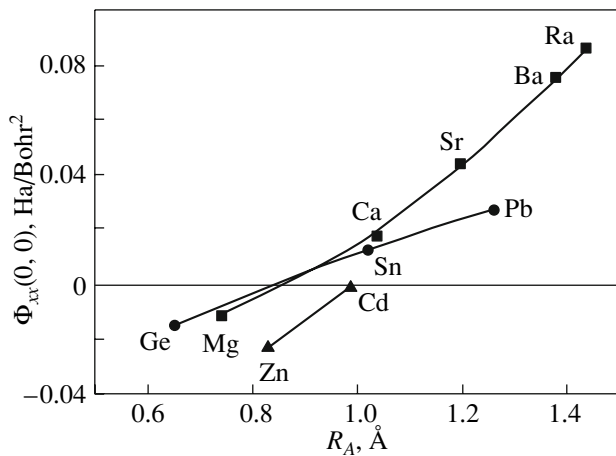
Fig. 2. Dependence of the diagonal matrix element $\Phi_{xx}(0, 0)$ of the A atom on its ionic radius.

Pb atoms in SrTiO$_3$ and BaTiO$_3$ can be in such positions [36].

The results of this study differ somewhat from the calculations carried out by Kvyatkovskiĭ [11], according to which an adiabatic multiwell potential arises only for Mg and Zn atoms, whereas Cd atoms remain at their sites. The discrepancy is likely due to the fact that the calculations in [11] were performed for a relatively small clusters in which the correlation of atomic motions cannot be correctly taken into account (the correlation length can be as large as 20 Å [5, 8]).

6. CONCLUSIONS

Pseudopotentials have been constructed and employed to calculate the phonon spectra of ATiO$_3$ perovskite crystals using the density functional theory. We have reproduced all known results concerning the structural instability of these crystals and predicted the properties of new, poorly studied systems. By analyzing the phonon spectra, the force-constant matrix, and the eigenvectors of unstable TO phonons, we revealed the regularities of the variation in the contributions from the chain instability and off-center atoms to the appearance of ferroelectricity in these crystals. The main factors determining the possible transfer of the A atoms to an off-center position are the geometric size of these atoms and the configuration of their outer electronic shell.

REFERENCES

1. R. E. Cohen and H. Krakauer, Phys. Rev. B: Condens. Matter **42**, 6416 (1990).

2. R. E. Cohen, Nature (London) **358**, 136 (1992).

3. W. Zhong, R. D. King-Smith, and D. Vanderbilt, Phys. Rev. Lett. **72**, 3618 (1994).

4. R. D. King-Smith and D. Vanderbilt, Phys. Rev. B: Condens. Matter **49**, 5828 (1994).

5. R. Yu and H. Krakauer, Phys. Rev. Lett. **74**, 4067 (1995).

6. C. LaSota, C.-Z. Wang, R. Yu, and H. Krakauer, Ferroelectrics **194**, 109 (1997).

7. U. V. Waghmare and K. M. Rabe, Phys. Rev. B: Condens. Matter **55**, 6161 (1997).

8. Ph. Ghosez, X. Gonze, and J.-P. Michenaud, Ferroelectrics **206–207**, 205 (1998).

9. Ph. Ghosez, E. Cockayne, U. V. Waghmare, and K. M. Rabe, Phys. Rev. B: Condens. Matter **60**, 836 (1999).

10. S. V. Halilov, M. Fornari, and D. J. Singh, Appl. Phys. Lett. **81**, 3443 (2002).

11. O. E. Kvyatkovskiĭ, Fiz. Tverd. Tela (St. Petersburg) **44** (6), 1087 (2002) [Phys. Solid State **44** (6), 1135 (2002)].

12. V. V. Lemanov, in *Defects and Surface-Induced Effects in Advanced Perovskites*, Ed. by G. Borstel, A. Krumins, and D. Millers (Kluwer, Dordrecht, The Netherlands, 2000), p. 329.

13. E. Cockayne and B. P. Burton, Phys. Rev. B: Condens. Matter **62**, 3735 (2000).

14. K. Parlinski, Y. Kawazoe, and Y. Waseda, J. Chem. Phys. **114**, 2395 (2001).

15. X. Gonze, J.-M. Beuken, R. Caracas, F. Detraux, M. Fuchs, G.-M. Rignanese, L. Sindic, M. Verstraete, G. Zerah, F. Jollet, M. Torrent, A. Roy, M. Mikami, Ph. Ghosez, J.-Y. Raty, and D. C. Allan, Comput. Mater. Sci. **25**, 478 (2002).

16. J. P. Perdew and A. Zunger, Phys. Rev. B: Condens. Matter **23**, 5048 (1981).

17. A. M. Rappe, K. M. Rabe, E. Kaxiras, and J. D. Joannopoulos, Phys. Rev. B: Condens. Matter **41**, 1227 (1990).

18. N. J. Ramer and A. M. Rappe, Phys. Rev. B: Condens. Matter **59**, 12471 (1999).

19. H. J. Monkhorst and J. D. Pack, Phys. Rev. B: Solid State **13**, 5188 (1976).

20. P. Giannozzi, S. Gironcoli, P. Pavone, and S. Baroni, Phys. Rev. B: Condens. Matter **43**, 7231 (1991).

21. X. Gonze, Phys. Rev. B: Condens. Matter **55**, 10337 (1997).

22. X. Gonze and C. Lee, Phys. Rev. B: Condens. Matter **55**, 10355 (1997).

23. D. R. Hamann, X. Wu, K. M. Rabe, and D. Vanderbilt, Phys. Rev. B: Condens. Matter **71**, 035117 (2005).

24. X. Gonze, J.-C. Charlier, D. C. Allan, and M. P. Teter, Phys. Rev. B: Condens. Matter **50**, 13035 (1994).

25. Landolt–Börnstein: Numerical Data and Functional Relationships in Science and Technology—New Series: Group III (Springer, Berlin, 1971), Vol. 6.

26. R. D. King-Smith and D. Vanderbilt, Phys. Rev. B: Condens. Matter **47**, 1651 (1993).

27. J. L. Servoin, Y. Luspin, and F. Gervais, Phys. Rev. B: Condens. Matter **22**, 5501 (1980).

28. T. Nakamura, Ferroelectrics **137**, 65 (1992).

29. R. A. Cowley, Phys. Rev. **134**, A981 (1964).

30. G. Fabricius and A. López Garcia, Phys. Rev. B: Condens. Matter **66**, 233 106 (2002).

31. Y. J. Shan, H. Mori, R. Wang, W. Luan, H. Imoto, M. Itoh, and T. Nakamura, Ferroelectrics **259**, 85 (2001).

32. Y. J. Shan, H. Mori, K. Tezuka, H. Imoto, and M. Itoh, Ferroelectrics **284**, 107 (2003).

33. Y. Konishi, M. Ohsawa, Y. Yonezawa, Y. Tanimura, T. Chikyow, T. Wakisaka, H. Koinuma, A. Miyamoto, M. Kubo, and K. Sasata, Mater. Res. Soc. Symp. Proc. **748**, U3.13 (2003).

34. N. Sicron, B. Ravel, Y. Yacoby, E. A. Stern, F. Dogan, and J. J. Rehr, Phys. Rev. B: Condens. Matter **50**, 13 168 (1994).

35. V. Shuvaeva, Y. Azuma, K. Yagi, H. Terauchi, R. Vedrinski, V. Komarov, and H. Kasatani, Phys. Rev. B: Condens. Matter **62**, 2969 (2000).

36. A. A. Veligzhanin, A. I. Lebedev, V. V. Mischenko, I. A. Sluchinskaya, and A. A. Chernyshov, in *Abstract Book of the Fifth International Seminar on Ferroelastic Physics, Voronezh, Russia, 2006* (Voronezh, 2006), p. 52.

Translated by Yu. Epifanov